Journal of Hazardous Materials 183 (2010) 353–365

Contents lists available at ScienceDirect

Journal of Hazardous Materials

journal homepage: www.elsevier.com/locate/jhazmat

Environmental geochemistry of ancient volcanic ashes

F. Ruggieri [a], J. Saavedra [b], J.L. Fernandez-Turiel [a,*], D. Gimeno [c], M. Garcia-Valles [c]

[a] Institute of Earth Sciences J. Almera, ICTJA, CSIC, Sole i Sabaris s/n, Barcelona, Spain
[b] IRNASA, CSIC, Salamanca, Spain
[c] Department of Geochemistry, Petrology and Geological Prospecting, Faculty of Geology, University of Barcelona, Barcelona, Spain

ARTICLE INFO

Article history:
Received 11 February 2010
Received in revised form 8 July 2010
Accepted 9 July 2010
Available online 15 July 2010

Keywords:
Volcanic ash
Leaching
Trace elements
Glass
Water

ABSTRACT

Volcanic ashes from the Puna and surrounding Andean areas in northern Argentina show that sometimes volcanic ash deposits are very well preserved (up to several million years) and can remain a potential hazard for the environment in a similar way as current deposits. Eight ashes have been characterized by SEM–EDX and DRX, and their potential released geochemical fluxes were examined by using water and nitric acid batches, which are analyzed by ICP-OES, ICP-MS and ISE (F). Results demonstrate that water batch system is better medium than nitric acid for this study. The high and fast reactivity of these ancient ashes is mainly associated with their high content in glass. The order of magnitude of released contents of implied elements is consistent among the samples, i.e., Al > B > Fe > Zn > F > P > Mn > Ba > Sr > Li > Ti > Rb > Cu > Ni > Sb > Pb > As > Cr > V. Ash–water interaction, although infrequent in arid regions such as the Puna Region in northern Argentina, introduces rapid changes in the geochemical fluxes of elements and pH and may constitute a potential hazard for the environment. In fact, many of these elements are included in the drinking water guidelines due to their potential toxicity and may constitute potential hazards for the environment and human health.

1. Introduction

During a volcanic eruption, magma, gas, and tephra are expelled from the volcanic vent into the atmosphere. Tephra are solid fragmented volcanic products which are classified according to the fragment size. Fragments less than 2 mm in diameter are termed ash, those between 2 and 64 mm are called lapilli, and fragments larger than 64 mm are called blocks [1]. The relative abundance of these products depends on the explosiveness of the magma, a feature closely related to the magma composition. The more silica and volatile the magma, the more explosive the results and the more ash is produced. Magmas with high silica and volatile content are usually constrained to specific geological settings on the Earth, consequently, the areas with the most explosive volcanoes are well known (e.g., the Andes in South America).

Volcanic ash is the most widely distributed product of explosive volcanic eruptions, and areas hundreds of kilometres from an erupting volcano could receive ash falls. Explosive eruptions are capable of causing significant environmental repercussions, affecting simultaneously, many cycles in the Earth's system, impacting on water, soil and surface sediments [2]. An important reflection of volcanic activity is the natural contribution of chemical elements to the Earth's surface and some of them have high potential toxicity [2–6]. Although eruptions are short-lived, ashfall deposits can remain in the local environment from months to decades, and in some exceptional cases may be preserved for during millions of years. Consequently, the geochemical characterization of volcanic ashes is an important issue in the study of geochemical mass balance on the Earth's surface.

Volcanic plumes in the atmosphere are heterogeneous environments in which gases and particulate matter can coexist and interact in several ways. The principal gases released during volcanic activity are water, carbon dioxide, sulphur dioxide, hydrogen, hydrogen sulphide, carbon monoxide and hydrogen chloride, but there are also many other compounds involved [7]. Sulphur, halogen and metal compounds are removed from the atmosphere by various processes such as chemical reaction, dry and wet deposition, and adsorption onto the surface of ash. The adsorption of volatiles varies and SO_4^{2-}, Cl^- and F^- show preferential enrichment on tephra surfaces [8]. Up to 40% of sulphur species and 10–20% of HCl can be scavenged by tephra in eruption columns [2,9–11]. Acids, salts and adsorbed gases on a tephra surface are highly soluble, dissolving rapidly in contact with water and inducing rapid biogeochemical changes upon deposition [12]. These compounds—acids, salts and adsorbed gases— make the ash little corrosive and potentially conductive. These soluble surface accumulations usually correspond to the leachable fraction of the ash [6]. Chemistry and volume of these products vary considerably.

* Corresponding author. Tel.: +34 93 409 54 10; fax: +34 93 411 00 12.
E-mail address: jlfernandez@ictja.csic.es (J.L. Fernandez-Turiel).

0304-3894/$ – see front matter © 2010 Elsevier B.V. All rights reserved.
doi:10.1016/j.jhazmat.2010.07.032

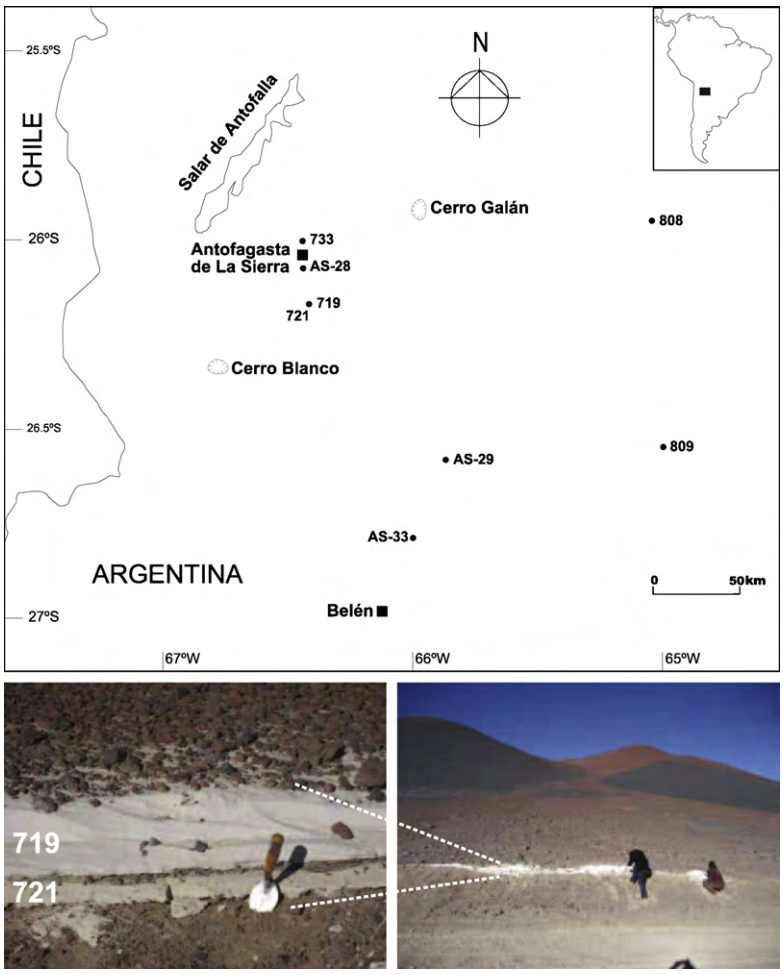

Fig. 1. Location of the sampling sites and photographs of the 719 and 721 ash deposits.

Though not representing the full complexity of a natural system, batch experiments are a feasible approach for the modelling of leachable ash fraction.

Volcanic ash leaching research focuses mainly on current eruptions around the world. The goal of this study is to characterize ancient volcanic ashes in order to determine their contribution to the local geochemical balance once they interact with water. To reach this objective, this study describes research done on ash deposits from the Andean region of the Puna in Northwestern Argentina (Fig. 1). The study area has been one of the most affected region in the world by explosive volcanism worldwide over the past several million years. This region has some of the largest and most explosive supervolcanoes in the world (e.g., Cerro Galán, Cerro Blanco). Many of the ash deposits of the Puna are extremely well preserved because of the hyper-arid conditions which are prevailing in the region for millions of years [13,14].

2. Geological setting

The Andean Cordillera consists of a >7500 km long morphologically continuous mountain chain along the western margin of South America. It is segmented into regions with distinct pre-Andean basement ages, Mesozoic and Cenozoic evolution, crustal thickness, structural trends, active tectonics, and volcanism. In general, subduction of the oceanic Nazca and Antarctica plates beneath the continental South American plate are responsible for the formation of magmas and volcanic processes along the western edge of South America. Three linear zones of active volcanism are present along the Andean Cordillera: the northern volcanic zone (NVZ: 12° N–5° S) located in Colombia and Ecuador; the central volcanic zone (CVZ: 5–33° S) primarily in south Peru and north Chile, but extending from east into southwestern Bolivia and northwestern Argentina; and the southern volcanic zone (SVZ: 33–56 °S) in southern Chile and southern Argentina.

In the central Andes, the Cordillera Occidental and the Cordillera Oriental flank the Altiplano-Puna plateau, an area which, from upper Miocene to Pleistocene, hosted several large-volume explosive eruptions which resulted in the deposition of extensive ignimbrites and volcanic ashes [15,16]. In addition, the CVZ is composed of eruptive products of calderas, stratovolcanoes and monogenetic centres of Oligocene to present age. This elevated region (>4000 m) includes 44 active volcanic edifices, as well as more than 18 active minor centres and/or fields and at least six potentially active Quaternary large silicic ignimbrite centre and/or caldera systems located [14,15].

The principal magma source for the andesitic volcanoes of the CVZ derives from the partial melting of an asthenospheric wedge between the overriding continental South American plate and the descending oceanic Nazca plate [15,17].

Our study is concerned with the characterization of volcanic ashes from the southern Puna and neighbouring areas in the southern part of the CVZ (Catamarca, Salta and Tucuman provinces, Argentina). The study area is located between 25.5 and 26° S and between 65 and 67° W (Fig. 1).

Table 1a
General features of the studied volcanic ashes from the Puna in Northwestern Argentina: coordinates of sampling sites (geodetic reference WGS 84), ashfall deposit thickness, mineral composition (***, common; **, frequent; *, scarce; w, rare; nd, not detected), Specific Surface Area (SSA), and bulk geochemistry (major oxides as %, m/m). LOI, loss on ignition; A/CNK, alumina saturation index.

Sample	719	721	733	808	809	AS-28	AS-29	AS-33
Latitude	67°23′47″W	67° 23′47″W	67°25′39″W	65°44′31″W	65°40′34″W	67°25′41″W	66°44′19″W	66°53′47″W
Longitude	26°18′52″S	26°18′52″S	26°02′39″S	25°57′00″S	26°55′56″S	26°09′19″S	26°58′40′S	27°19′31″S
Height (m)	3144	3144	3371	1473	1883	3328	2471	3328
Deposit thickness (cm)	30	10	30	25	450	35	50	40
Glass	***	***	***	***	***	***	*	*
Quartz	**	***	*	nd	*	**	**	**
Albite	***	*	**	nd	*	**	**	**
Sanidine	**	*	**	nd	*	**	*	*
Biotite	*	**	**	nd	w	**	w	w
Cristobalite	nd	w	nd	nd	nd	w	*	*
SSA ($m^2\ g^{-1}$)	0.55	1.12	1.31	7.74	1.49	0.99	2.28	4.82
SiO_2	74.55	72.08	73.72	69.79	73.10	72.52	68.30	68.74
Al_2O_3	12.45	12.61	12.77	14.25	12.82	13.26	14.92	14.52
Fe_2O_3	0.81	2.01	0.93	0.99	0.89	1.08	2.87	3.15
MgO	0.16	0.77	0.32	0.42	0.22	0.32	0.92	0.92
CaO	0.89	1.65	0.92	0.81	0.71	1.03	2.82	2.99
Na_2O	3.92	3.60	3.68	4.20	4.18	4.22	4.23	4.03
K_2O	4.49	4.11	4.70	4.29	4.44	4.46	3.49	3.07
TiO_2	0.11	0.26	0.13	0.14	0.12	0.14	0.32	0.35
P_2O_5	0.02	0.06	0.03	0.05	0.01	0.02	0.10	0.08
LOI	2.57	2.79	2.77	4.98	3.42	2.90	2.00	2.13
Total	99.96	99.94	99.97	99.91	99.92	99.94	99.97	99.96
Si/Al molar	5.08	4.85	4.90	4.16	4.84	4.64	3.88	4.02
A/CNK	0.96	0.94	1.00	1.09	0.99	0.97	0.94	0.94

3. Materials and methods

3.1. Sampling

Eight volcanic ash deposits were sampled in the southern Puna and neighbouring areas throughout the period 2006–2007. Sampling sites were marked by GPS and the coordinates are plotted in Table 1a. Ash layers were identified by considering the local geological setting, the morphology of the layered deposit, the grain size of the sediment (fine sand to silt) and the colour (gray, cream and white). By taking into account their stratigraphic position, the age of these deposits was constrained to hundreds of thousands to several million years [18]. Samples were collected by a stainless steel shovel excluding the most superficial (2 cm depth) ash. About 2 kg of sample were placed in polyethylene bags and carried to the laboratory. Samples were dried at 40 °C in an oven and stored in polyethylene vessels until preparation in the laboratory.

3.2. Physical and mineralogical characterization

Brunauer–Emmett–Teller (BET) analysis can provide reliable information regarding textural features such as the Specific Surface Area (SSA) of a particular specimen. For the present study, SSA analysis was conducted by applying a gravimetric nitrogen BET specific surface analysis technique using a Micromeritics ASAP 2010, an automatic physisorption analyzer with multi-gas option. All analyses were performed with N_2 as the adsorbate gas at liquid nitrogen temperature (≈77° K). To improve analysis accuracy, the ASAP 2010 has a high vacuum molecular drag pump capable of producing a vacuum of 10^{-5} mmHg or better, 1000 and 10 mmHg pressure transducers, completely independent vacuum systems for sample outgassing and analysis, and isothermal jackets to maintain constant sample temperature throughout the determination. The instrument was calibrated using both high ($216 \pm 6\ m^2\ g^{-1}$) and low ($0.61 \pm 0.08\ m^2\ g^{-1}$) silica–alumina surface area standards. Prior to the determination of the adsorption isotherm, the sample was evacuated while heating at 90 °C for 1 h and then at 350 °C for at least 4 h. This procedure assures complete outgassing of the finer pores that may contribute substantially to the total SSA of porous materials. BET estimates of surface areas were based on isotherms with at least five points in the linear range and correlation coefficients typically greater than 0.9999. The typical accuracy of SSA determinations based on the BET model is ±10%.

Scanning electron microscopy (SEM) is a fast and cost-effective analytical tool for the characterization of volcanic ashes. It facilitates the description of particle shape, vesicularity and external surface texture as well as the eventual occurrence of surface alteration or secondary minerals, and the particle size determination [19,20]. Moreover, the X-ray energy dispersive analyzer (EDX), currently coupled with SEM, helps to identify through a semi-quantitative chemical analysis the mineral phases associated with the glass shards [21]. Elements occurring in concentrations of 1% (m/m) and even less are readily detectable. However, there are two requirements for samples studied by SEM–EDX as they must be dry and conductive. For this study, volcanic ash samples were dried in an oven at 40 °C prior to being mounted on carbon stubs and coated with carbon in a vacuum evaporator. SEM images and spot EDX analyses were performed using a FEI Quanta 200 instrument equipped with a Genesi program and an EDX detector (minimum spot size: 5 μm; working distance: 10 mm; accelerating voltage: 20 kV).

The mineralogical characterization was carried out by X-ray diffraction (XRD) analysis. Samples were powdered in an agatha mortar and diffractograms were obtained using a Bruker D-5005 instrument (CuKα1 radiation, λ = 1.5406 Å, at 40 kV and 40 mA), which collects data between 4 to 60° of 2θ, with a scan step of 0.05° and a step duration of 3 s. Evaluation of diffractogram was carried out by using DIFFRAC software.

3.3. Bulk chemical analysis

Samples were ground in a laboratory vibrating disc mill of tungsten carbide. This mill set contaminates the sample with tungsten. Concentrations of major elements in volcanic ashes were determined by inductively coupled plasma optical emission spectrometry (ICP-OES, Optima 3100×, PerkinElmer), and trace elements by inductively coupled plasma mass spectrometry (ICP-MS, Elan 6000, PerkinElmer), except for SiO_2, Y, Zr and Nb which were

Table 1b
Concentration ($\mu g\,g^{-1}$) of trace elements in the studied volcanic ashes.

Sample	719	721	733	808	809	AS-28	AS-29	AS-33
Li	90.31	93.23	86.39	56.77	111.48	93.67	12.49	17.29
Be	6.35	6.39	6.52	3.31	6.75	6.29	2.35	2.02
V	6.60	33.06	8.84	8.19	6.17	8.59	52.99	62.59
Cr	4.49	21.24	11.17	4.44	3.73	6.95	17.24	21.17
Mn	593.44	695.28	572.30	661.03	651.88	667.24	463.99	451.40
Co	0.82	4.39	1.86	23.42	12.56	27.26	19.38	32.68
Ni	2.52	11.44	5.82	3.04	1.84	5.10	12.32	9.15
Cu	7.13	9.55	4.38	5.17	4.62	7.03	12.82	10.90
Zn	39.86	60.31	41.97	53.80	39.85	111.13	71.88	56.33
Ga	20.22	21.35	20.04	18.60	21.09	20.35	20.95	19.63
Ge	1.84	1.92	1.85	1.50	1.94	2.07	0.90	0.75
As	5.75	7.37	5.46	6.34	6.69	7.24	1.44	1.35
Rb	375.83	347.73	372.84	145.71	400.63	494.58	132.99	81.25
Sr	24.62	93.62	41.69	90.30	25.72	37.31	354.48	482.40
Y	17.51	20.07	17.76	16.10	19.63	17.90	11.72	11.37
Zr	68.52	89.70	72.60	78.70	57.83	66.20	22.08	80.00
Nb	32.99	33.29	29.99	10.26	27.76	27.11	14.77	7.75
Mo	2.68	2.81	2.78	2.60	2.89	2.86	1.86	0.22
Sn	2.71	6.91	3.63	2.34	3.61	3.71	2.24	1.81
Sb	1.13	1.20	1.14	0.31	1.18	2.40	9.11	2.71
Cs	25.13	24.39	25.25	4.97	27.84	26.88	6.78	2.71
Ba	34.95	152.68	61.89	819.98	41.27	69.57	439.40	578.09
La	14.51	22.09	18.01	17.66	18.69	17.47	73.82	50.90
Ce	33.69	45.84	37.92	37.08	39.80	37.28	113.13	84.02
Pr	10.65	5.40	4.42	4.23	4.64	4.24	10.76	8.46
Nd	12.73	19.31	15.29	14.47	16.01	14.69	33.39	27.87
Sm	5.26	4.00	3.18	3.12	3.36	3.10	4.82	4.30
Eu	0.79	0.48	0.30	0.56	0.26	0.29	1.23	1.07
Gd	2.48	3.96	3.17	3.16	3.33	3.07	6.08	4.79
Tb	0.96	0.60	0.49	0.52	0.52	0.48	0.65	0.54
Dy	2.39	3.57	2.98	3.13	3.18	2.97	3.52	2.99
Ho	1.00	0.67	0.57	0.57	0.63	0.58	0.55	0.47
Er	1.55	2.17	1.88	1.71	2.04	1.88	1.88	1.51
Tm	0.59	0.34	0.30	0.25	0.33	0.30	0.25	0.20
Yb	1.77	2.50	2.19	1.68	2.39	2.22	1.67	1.32
Lu	0.70	0.38	0.35	0.25	0.38	0.36	0.24	0.19
Hf	3.48	4.54	3.73	3.50	4.33	3.94	2.18	1.06
Ta	2.01	2.01	1.63	0.57	1.63	1.94	0.77	0.45
Tl	1.98	1.81	1.93	0.82	1.96	1.76	0.75	0.32
Pb	36.48	35.54	36.64	25.28	36.73	39.18	21.71	18.10
Bi	1.17	1.18	1.24	0.31	1.28	1.10	0.27	0.14
Th	29.10	27.05	28.17	13.18	29.32	31.87	32.20	19.16
U	18.27	17.26	18.45	4.21	19.90	24.41	6.08	4.05

determined by X-ray fluorescence spectrometry (XRF). Whole-rock analysis by ICPs was performed on a split (0.1 g) of each sample. It was digested with HNO_3:$HClO_4$:HF (2.5:2.5:5 ml, v/v), doubly evaporated to incipient dryness by adding HNO_3, and finally volume was made up to 100 ml with 1% (v/v) HNO_3. Loss on ignition (LOI) was determined on a 1 g sample at 1000 °C. This sample preparation procedure is not efficient for all elements due to the fact that, for instance, Y, Zr and Nb-bearing minerals are resistant to the digestion; Si, Cl, S, B, F, Br, and Hg are lost by volatilization; and others, such as CI, interfere when applying ICP-MS to certain analytes (e.g., As and V). Consequently, Si, Y, Zr and Nb were analyzed by XRF whereas the others were only studied in leachates.

For silica analysis by XRF, 0.1 g of sample was mixed with a Na_2O_2 flux and fused (450 °C for 30 min). The product was then poured into a mould to obtain a homogenous fused disc. For the analysis of Y, Zr and Nb, about 5 g of powdered sample were placed in an oven at 90 °C for at least 12 h. Then, they were mixed with 2 ml of Elvacite 2044 diluted in acetone (20% solution) in an agatha mortar, until a homogeneous powder was obtained. The bottom of an aluminium dish was filled with boric acid (powder) and the sample

Table 2a
Raw water batch geochemistry (0.1 g ash in 5 ml water). Concentrations as $mg\,l^{-1}$.The pH was monitored in duplicate batches at the beginning (pH_0), immediately after ash–water mixing, and at the end of the experiment (pH_f), without filtering.

Parameter	719	721	733	808	809	AS-28	AS-29	AS-33
pH_0	8.09	8.03	8.15	7.08	8.53	8.55	8.59	8.47
pH_f	7.64	7.23	7.46	7.27	8.07	7.87	8.02	7.97
Ca	14.71	16.08	4.91	4.97	6.02	10.25	11.03	10.23
Mg	0.12	0.39	0.23	0.29	0.48	0.25	4.20	2.56
Na	6.75	2.45	15.21	48.55	18.08	2.53	4.91	20.69
K	3.27	4.61	5.22	5.08	3.22	4.25	7.94	12.05
Si	8.12	13.41	12.64	12.85	9.63	9.39	54.55	39.40
Cl	3.22	3.31	2.18	50.75	11.94	10.24	2.82	2.27
SO_4	1.08	7.83	1.08	10.64	15.29	1.08	12.95	2.15
HCO_3	69.33	12.64	66.03	52.51	33.75	28.97	58.77	111.07
Si/Al molar	11.41	15.54	13.52	5.93	9.33	14.18	10.08	2.55

Table 2b
Raw water batch geochemistry (0.1 g ash in 5 ml water): trace elements. Concentrations expressed as $\mu g\,l^{-1}$.

Sample	719	721	733	808	809	AS-28	AS-29	AS-33
Li	13.52	16.97	10.07	30.30	76.61	9.69	8.07	16.67
Be	0.01	0.01	0.07	0.39	0.01	0.01	0.54	1.08
F	101.20	107.70	26.70	62.50	966.00	59.40	42.60	42.60
B	354.49	190.79	420.18	417.66	328.24	335.94	285.52	346.09
Al	683.65	828.73	898.38	2079.41	992.16	636.06	5198.41	14825.51
P	61.03	696.79	874.73	634.33	1400.00	415.91	204.00	2149.95
Ti	12.25	19.23	21.58	43.48	20.94	18.63	313.16	632.52
V	1.14	2.42	4.18	4.10	10.74	3.36	5.02	16.67
Cr	2.09	4.67	3.61	1.00	1.00	4.12	3.51	4.46
Fe	240.46	419.20	496.34	542.95	461.15	420.88	4188.63	5938.25
Mn	23.69	36.25	27.60	83.43	30.23	25.45	113.01	162.81
Co	0.39	0.55	1.35	22.65	0.42	3.69	71.27	158.82
Ni	3.42	6.06	4.58	6.57	4.90	6.97	6.69	10.50
Cu	4.89	9.41	5.62	15.07	12.86	10.69	11.34	17.15
Zn	169.49	989.13	98.29	138.33	121.53	269.41	261.18	129.61
Ga	0.22	0.27	0.34	0.44	0.40	0.17	1.97	5.37
Ge	0.05	0.03	0.01	0.14	0.10	0.01	0.18	0.26
As	2.17	4.08	0.08	0.41	1.89	15.51	0.04	2.03
Br	<0.05	<0.05	<0.05	10.7	46.68	<0.05	<0.05	<0.05
Rb	7.14	8.70	7.22	7.46	4.04	3.40	23.78	47.40
Sr	14.42	56.76	14.31	28.15	6.48	16.71	47.08	136.70
Y	0.32	0.80	0.75	1.41	1.31	0.59	1.37	3.74
Zr	0.57	0.91	0.28	4.13	1.68	1.89	4.15	4.36
Nb	0.57	0.42	0.31	1.08	1.23	0.35	3.29	4.02
Mo	0.59	0.96	0.89	1.36	2.27	1.09	1.23	0.97
Sn	<0.01	0.44	<0.01	<0.01	<0.01	<0.01	<0.01	<0.01
Sb	2.86	3.41	2.14	3.26	3.02	2.13	3.11	2.48
Cs	0.27	0.35	0.73	0.49	0.31	0.19	1.25	3.63
Ba	14.62	28.59	16.72	44.50	26.03	10.86	35.66	146.86
La	0.70	1.30	1.36	1.61	1.44	1.16	8.39	30.17
Ce	1.86	2.56	12.62	3.37	1.83	1.90	8.80	47.90
Pr	0.11	0.30	0.34	0.40	0.34	0.25	1.09	4.81
Nd	0.42	0.96	1.39	1.33	1.31	0.85	3.59	12.82
Sm	0.02	0.12	0.20	0.33	0.29	0.10	0.35	1.85
Eu	0.02	0.02	0.03	0.03	0.03	0.02	0.05	0.35
Gd	0.11	0.19	0.29	0.29	0.26	0.15	0.44	2.02
Tb	0.02	0.03	0.03	0.05	0.04	0.02	0.06	0.22
Dy	0.04	0.12	0.13	0.27	0.29	0.12	0.24	1.30
Ho	0.01	0.02	0.03	0.05	0.04	0.02	0.06	0.19
Er	0.05	0.07	0.07	0.11	0.10	0.06	0.16	0.56
Tm	0.00	0.00	0.01	0.01	0.01	0.02	0.03	0.09
Yb	0.04	0.05	0.07	0.14	0.13	0.05	0.18	0.57
Lu	0.00	0.01	0.00	0.02	0.01	0.01	0.03	0.09
Hf	0.23	0.35	0.13	0.70	1.05	0.74	0.56	0.97
Ta	0.11	0.07	0.06	0.25	0.19	0.09	0.40	0.90
Hg	1.06	0.46	0.31	2.09	0.24	0.38	16.19	16.30
Tl	0.00	0.00	0.03	0.07	0.02	0.00	0.17	0.29
Pb	2.21	4.17	2.75	6.88	4.76	5.20	3.85	13.51
Bi	<0.01	<0.01	<0.01	0.13	0.14	<0.01	<0.01	0.02
Th	0.10	0.10	0.10	0.24	0.27	0.10	1.44	3.89
U	0.19	0.39	0.18	0.13	0.48	0.16	1.10	2.86

with Elvacite powder was sprinkled over this boric acid layer. The dish was pressed and compacted using a Herzog press at a maximum pressure of 200 kN for 1 min. XRF analyses were performed using a Phillips PW2400 sequential spectrometer.

The precision and accuracy of analytical determinations were monitored using reference materials of the Geological Survey of Japan (rhyolite JR-3 and basalt JB-3) [22,23].

3.4. Batch leaching tests

Batch leaching experiments were performed on unground and unsieved ashes using deionized water and nitric acid. Batch testing is the simplest one-stage leaching procedure. The contact time used in such tests was considered long enough for chemical equilibrium to be established.

Table 3a
Raw nitric acid batch geochemistry (0.1 g ash in 1 ml HNO_3). Concentrations expressed as $mg\,l^{-1}$. S_n/S_w ratio, S in nitric batch to S in water batch.

Sample	719	721	733	808	809	AS-28	AS-29	AS-33
Ca	251.27	519.49	241.15	200.85	180.33	215.59	313.36	250.97
Mg	17.04	91.57	35.86	40.01	36.67	60.77	21.37	61.40
Na	22.17	32.08	48.14	279.79	165.87	37.74	85.94	305.28
K	25.92	41.42	45.09	66.22	39.05	53.32	54.53	288.39
Si	10.42	16.81	15.07	17.77	31.17	21.34	16.43	37.39
Cl	17.09	18.23	18.81	65.10	54.27	44.61	26.84	28.53
SO_4	379.77	383.26	330.47	422.64	437.71	306.84	384.83	318.54
S_n/S_w	70.33	9.80	61.20	7.95	5.73	56.82	5.94	29.65

Table 3b
Raw nitric acid batch geochemistry (0.1 g ash in 1 ml HNO_3): trace elements. Concentrations expressed as $\mu g\,l^{-1}$.

Sample	719	721	733	808	809	AS-28	AS-29	AS-33
Li	154.75	268.24	163.35	539.91	1031.13	290.22	103.61	349.90
Be	5.13	7.39	5.97	35.50	5.41	8.97	16.57	7.60
B	513.30	439.69	495.11	619.69	881.07	846.62	562.77	673.92
Al	37108.30	55246.12	30128.11	171660.67	56849.23	71897.74	52190.93	216191.80
P	8848.36	16684.59	14333.74	11319.96	6458.86	6523.18	37019.80	37304.32
Ti	1306.01	1573.65	1147.13	474.40	4121.24	5489.97	2331.38	8725.91
V	35.84	152.62	77.30	108.08	176.40	179.70	118.62	286.18
Cr	27.00	87.16	44.32	90.44	99.03	122.47	42.43	91.10
Fe	25475.01	82154.70	36470.41	29946.26	62691.45	111918.66	34905.36	115775.45
Mn	2419.68	5450.31	1908.15	9059.33	4292.28	5470.14	2237.25	3994.98
Co	19.98	80.04	94.08	2165.93	33.83	57.22	1291.22	2687.44
Ni	232.79	570.56	373.04	238.83	162.00	277.13	237.81	294.07
Cu	129.92	239.30	121.42	113.24	207.55	192.53	83.57	220.82
Zn	3953.15	4722.34	4354.59	3497.21	3970.00	4417.23	2619.97	3680.69
Ga	14.26	23.62	13.10	28.79	26.09	35.21	21.36	84.97
Ge	0.01	0.08	0.01	0.71	0.69	0.27	0.19	1.14
As	100.97	179.08	100.23	122.75	54.88	211.79	90.05	110.91
Br	1005.28	886.34	828.53	70.74	118.38	1630.69	1271.33	1210.90
Rb	286.10	411.50	258.90	280.50	335.60	538.00	699.50	1602.10
Sr	499.58	1223.58	551.45	1705.20	467.22	377.41	413.36	2253.42
Y	39.84	141.96	60.88	146.52	74.49	85.10	109.51	139.97
Zr	39.16	70.91	34.04	86.77	66.91	55.22	81.41	123.89
Nb	5.24	4.02	2.96	7.85	11.39	13.21	9.11	5.04
Mo	45.38	40.51	38.26	30.75	46.44	41.12	33.95	23.45
Sn	< 0.01	< 0.01	< 0.01	6.05	6.20	1.88	< 0.01	0.19
Sb	13.00	8.33	8.69	13.56	16.97	11.11	11.62	10.60
Cs	24.04	34.89	44.16	38.36	17.56	37.71	48.73	143.66
Ba	674.44	1881.05	1079.70	4793.59	534.57	350.76	520.11	2487.71
La	56.04	224.06	126.98	152.85	122.13	141.02	575.86	1008.81
Ce	117.42	454.88	259.07	369.83	234.19	291.07	876.58	1588.13
Pr	14.78	60.46	33.34	40.25	28.85	35.75	89.06	146.51
Nd	57.78	237.52	125.14	147.44	110.78	139.50	266.47	458.52
Sm	11.61	46.20	23.06	32.45	20.40	27.38	32.46	59.81
Eu	1.56	6.83	3.39	5.49	3.07	3.80	4.29	8.50
Gd	10.78	46.20	22.64	32.55	21.11	25.59	39.44	67.22
Tb	1.53	6.04	2.74	5.40	2.91	3.27	3.81	6.61
Dy	8.09	31.86	13.99	29.55	14.85	18.45	20.74	31.46
Ho	1.31	5.05	2.05	5.08	2.43	2.87	3.29	4.34
Er	3.83	14.09	5.73	14.88	6.89	8.52	10.35	13.47
Tm	0.53	1.74	0.66	1.99	0.90	0.87	1.43	1.58
Yb	3.35	9.90	4.08	14.16	5.57	5.76	9.85	10.73
Lu	0.45	1.43	0.58	1.93	0.76	0.77	1.46	1.67
Hf	3.24	5.43	2.68	21.56	35.72	6.77	5.78	7.27
Ta	0.37	0.33	0.31	2.01	1.61	0.40	0.47	0.82
Hg	1.42	0.86	0.84	45.72	3.54	0.52	43.03	33.12
Tl	1.42	3.66	2.18	2.14	2.97	5.84	1.92	7.90
Pb	90.52	131.39	86.16	302.92	106.88	130.77	43.79	302.25
Bi	2.99	2.65	2.56	2.12	2.67	3.29	2.01	3.57
Th	31.71	53.74	21.06	55.96	36.59	35.54	223.73	146.77
U	8.61	17.97	5.64	9.88	13.59	8.34	47.10	25.07

For water batch experiments, 0.1 g of ash was mixed with 5 ml MilliQ Q Plus type deionized water (18.2 $M\Omega\,cm^{-1}$) in 14 mm × 100 mm polypropylene test tubes. After 12 h of stirring at 20 rpm at room temperature, the leached solutions were filtered through cellulose nitrate membranes (Whatman, 0.45 μm pore size, 142 mm diameter) and the volume was made up to 100 ml in 1% (v/v) HNO_3. Following this methodological approach, new batches were also prepared using 1 ml HNO_3 as leaching agent. In addition to the elements analyzed in the whole-rock analysis, Cl, S, B, Br, and Hg concentrations were analyzed in the batch samples. Given the physico-chemical characteristics of the samples studied, the Cl, Br, and S concentrations were expressed as Cl^-, Br^-, and SO_4^{2-}, respectively. The methods to determine major and trace elements using ICP-MS analysis were described previously [24–26]. Furthermore, the fluoride concentrations were determined by ISE (Orion, Thermo Scientific), but only in water batches, and concentrations of HCO_3 were modelled in water batches using Geochemical Workbench (GWB 8.0.2) software [27].

The water leachate pH was monitored in duplicate batches immediately after ash–water mixing and at the end of the experiment, without filtering.

3.5. Data presentation

Table 1a shows the mineralogical composition, the SSA values and the bulk geochemistry (major and trace elements) of the studied samples. Tables 2a and 2b and Tables 3a and 3b present the contents of those elements solubilised in water and nitric acid batches. Tables 4 and 5 display the relative mass leached factors (RML) for water and nitric acid batches, respectively. The RML is defined as the fraction, expressed as %, of leached element (element/solid by weight) obtained from the batch leaching tests (i.e., water batch test and nitric acid batch tests) over the total element concentration (element/solid by weight) obtained from the total elemental analysis [28,29]. Although Se, Ag, Cd, Te, Pt, and Au were analyzed, however, these could not be studied because their concentrations were below or very close to the respective detec-

Table 4
Relative mass leached factors or RMLs (%) in water batches (nd, not determined).

Sample	719	721	733	808	809	AS-28	AS-29	AS-33
Ca	11.37	6.00	3.72	4.27	5.18	6.69	2.67	2.32
Mg	0.61	0.37	0.60	0.56	1.61	0.62	3.68	2.24
Na	1.14	0.41	2.77	7.74	2.55	0.39	0.76	3.36
K	0.43	0.60	0.66	0.71	0.38	0.55	1.34	2.29
Si	0.11	0.18	0.18	0.20	0.12	0.13	0.83	0.59
Li	0.74	0.80	0.58	2.65	3.01	0.50	3.16	4.67
Be	0.01	0.01	0.05	0.59	0.01	0.01	1.13	2.59
Al	0.05	0.05	0.07	0.14	0.06	0.04	0.32	0.93
P	3.33	12.02	29.46	15.25	95.69	29.02	2.33	28.59
Ti	0.10	0.05	0.14	0.26	0.13	0.11	0.80	1.48
V	0.85	0.32	2.34	2.49	7.64	1.88	0.46	1.29
Cr	2.30	0.97	1.60	1.12	1.17	2.85	0.99	1.02
Fe	0.21	0.13	0.38	0.39	0.33	0.27	1.02	1.31
Mn	0.20	0.23	0.24	0.63	0.20	0.18	1.19	1.75
Co	2.33	0.55	3.61	4.81	0.15	0.65	17.96	23.55
Ni	6.70	2.34	3.91	10.74	11.69	6.57	2.65	5.56
Cu	3.38	4.35	6.36	14.48	12.21	7.31	4.32	7.62
Zn	20.95	72.38	11.62	12.78	13.38	11.67	17.74	11.15
Ga	0.05	0.06	0.08	0.12	0.08	0.04	0.46	1.33
Ge	0.14	0.07	0.03	0.45	0.22	0.01	0.98	1.65
As	1.86	2.44	0.07	0.32	1.24	10.31	0.14	7.26
Rb	0.09	0.11	0.10	0.25	0.04	0.03	0.87	2.83
Sr	2.89	2.68	1.70	1.55	1.11	2.16	0.65	1.37
Y	0.09	0.18	0.21	0.44	0.29	0.16	0.57	1.59
Zr	0.04	0.04	0.02	0.26	0.13	0.14	0.92	0.26
Nb	0.08	0.06	0.05	0.52	0.19	0.06	1.09	2.51
Mo	1.08	1.51	1.59	2.59	3.44	1.83	3.22	21.59
Sn	nd	0.28	nd	nd	nd	nd	nd	nd
Sb	12.41	12.51	9.27	51.98	11.17	4.27	1.67	4.44
Cs	0.05	0.06	0.14	0.49	0.05	0.03	0.90	6.48
Ba	2.06	0.83	1.34	0.27	2.77	0.75	0.40	1.23
La	0.24	0.26	0.37	0.45	0.34	0.32	0.55	2.87
Ce	0.27	0.25	1.65	0.45	0.20	0.24	0.38	2.76
Pr	0.05	0.24	0.38	0.47	0.32	0.28	0.49	2.75
Nd	0.16	0.22	0.45	0.46	0.36	0.28	0.53	2.23
Sm	0.02	0.13	0.31	0.53	0.38	0.16	0.36	2.09
Eu	0.13	0.22	0.47	0.23	0.53	0.30	0.21	1.57
Gd	0.21	0.21	0.45	0.46	0.35	0.24	0.35	2.04
Tb	0.10	0.25	0.35	0.46	0.37	0.24	0.42	2.00
Dy	0.09	0.15	0.22	0.43	0.40	0.19	0.34	2.11
Ho	0.05	0.16	0.24	0.40	0.31	0.15	0.51	1.91
Er	0.17	0.14	0.17	0.32	0.21	0.16	0.43	1.80
Tm	0.02	0.03	0.13	0.16	0.13	0.28	0.51	2.17
Yb	0.10	0.09	0.15	0.42	0.23	0.12	0.53	2.08
Lu	0.03	0.07	0.06	0.40	0.16	0.16	0.64	2.38
Hf	0.33	0.34	0.17	1.00	1.06	0.91	1.25	4.43
Ta	0.27	0.15	0.18	2.17	0.51	0.23	2.57	9.66
Tl	0.01	0.01	0.09	0.41	0.04	0.01	1.09	4.40
Pb	0.30	0.52	0.37	1.35	0.57	0.64	0.87	3.62
Bi	nd	nd	nd	2.04	0.49	nd	nd	0.55
Th	0.02	0.02	0.02	0.09	0.04	0.02	0.22	0.98
U	0.05	0.10	0.05	0.15	0.11	0.03	0.88	3.42

tion limits. RMLs were not determined for Cl, SO_4, B, F, Br, and Hg because these elements were not analyzed in bulk ashes.

Once determined the RMLs for each element and for each leaching method, then the elements were grouped informally according to their mobility, expressed by their RML: for example, high mobility for elements showing RML >5% or even more, moderate mobility for elements with RML between 0.5 and 5%, and low mobility for those elements having RML <0.5%. The low mobility group shows a low potential hazard for the environment [29].

4. Results and discussion

4.1. Ash characterization

The studied ashes are rhyolites (70–77%, SiO_2, m/m) according to the Total Alkali Silica (TAS) diagram for the classification of volcanic rocks [30]. In a first approach, the characterization based on SEM and DRX analysis showed that glass is the main constituent of all types of ash, though there are also minor amounts of quartz, albite, sanidine and biotite (Table 1a). The presence of cristobalite is remarkable in samples 721 and AS-28. This mineral was observed as highly crystalline silica nanofibers in the respirable fraction of the unaltered volcanic ash of the Chaiten Volcano Eruption in 2008 (Southern Andes, Chile), and interpreted as generated during explosive eruptions by the reduction of amorphous silica by carbon monoxide to its reactive suboxide SiO, which was later oxidized to form one-dimensional crystalline silica nanostructures [31]. Cristobalite has also been found in the andesite lava dome of the Soufriere Hills volcano, Montserrat [32]. This finding perhaps could help to fingerprint ancient explosive eruptions similar to the ongoing lava dome explosive eruptions in the Chaiten and the Soufriere Hills volcanoes. In the current case at hand, samples No. 721 and AS-28 might have originated in eruptions of similar type.

The differences in mineral contents and morphological features (Fig. 2), mainly the grain-size distribution, allowed us to classify the samples into three broad groups of ashes: (1) ash (sample

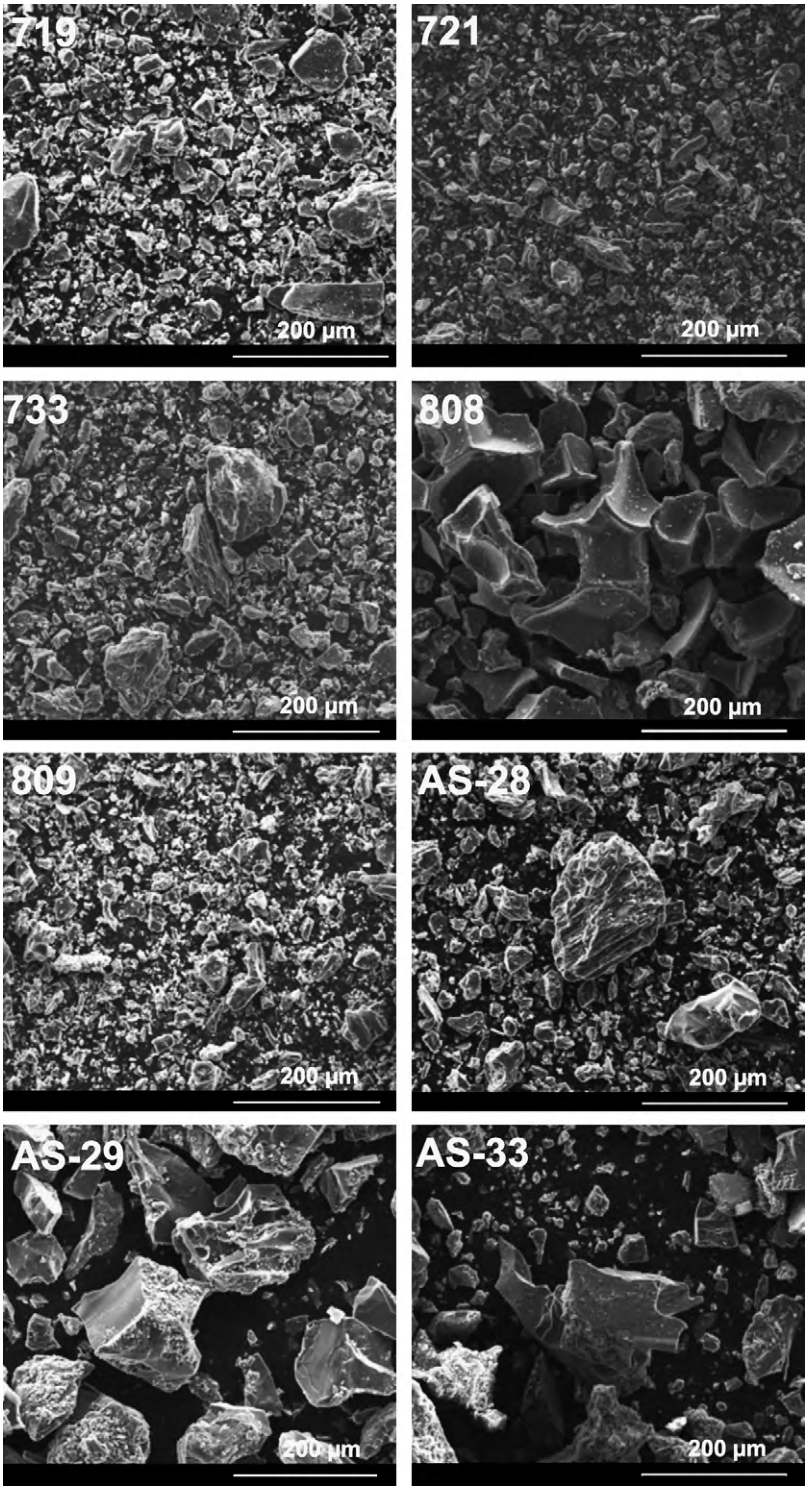

Fig. 2. SEM images of the studied volcanic ashes.

808) practically made up only of glass, with abundant Y-shaped, plate like, curved, and angular shards (typically from spherical vesicle wall breakage), with homogeneous grain-size distribution; (2) ashes (samples 719, 721, 809 and AS28) with crystalline phases and a significant glass content (irregular blocky fragments and, in some cases with parallel, highly elongated pipe-like vesicles parallel to the long axis of the pyroclast indicating the flow direction), and bimodal grain-size distribution, 10–100 μm particles coexist with abundant <5 μm particles; and (3) ashes (samples AS29 and AS33) with a high content of crystalline phases and rare fine grain-sized particles; the glass consisting of poorly vesicular equant blocky fragments.

These three groups fingerprint three different volcanic styles. The high content of glass in Group 1 indicates a highly explosive magma with practically no crystal, probably due to the fast ascent of the magma to the surface, whereas the high contents of fine (<5 μm) particles in Group 2 could indicate highly explosive eruptions, probably related to ongoing lava dome explosive eruptions in

the case of the cristobalite-bearing ashes (samples 721 and AS-28). Finally, Group 3 shows typical characteristics of explosive eruptions with possible magma stagnation in a chamber during the ascent, which provided the crystallization of the observed minerals.

Samples AS29 and AS33, although separated by ~50 km, are possibly from the same volcano and possibly from the same eruption. Their morphology, mineralogy, and chemical composition, both major oxides and trace elements (Tables 1a and 1b), seem to indicate that these two samples might have been collected from the same ashfall deposit although at different distances from the source volcano.

4.2. Water batch tests

Although the duration of the water batches was relatively short (12 h), the factors discussed in the following paragraphs indicate that the ash–water interaction must have been incipient but significant. This view is consistent with results by several authors who have found that the dissolution of glasses and other compounds occurring in volcanic ashes is remarkable even with shorter shaking times than the 12 h considered here [6]. In any case, these results should be taken as typical of an early stage of weathering.

4.2.1. pH and hydrolysis

The data in Table 2a indicate that immediately after adding deionized water (with a pH slightly acid) to the ash and before beginning the process of agitation for 12 h, the pH increased to weakly alkaline. It is evident that there can be no hydrolysis or generalized dissolution generating this change in such a short period of time.

Reactions of minerals with water and their thermodynamic fundamentals highlighted as pH changes are very common when mineral phases are contacted with water [33]. In the case of silica, the main constituent of glass, H^+ and $(OH)^-$ diffuse in the three spatial dimensions, even through the solid surface charge. In these active interfaces, the $(OH)^-$ are linked to Si and the H^+ to O, promoting the dissociation of water (the water dissociation constant, K_w, changes by several orders of magnitude in these conditions). This explains because the suspended solids in natural waters are often negatively charged at pH close to neutrality (6–8). Although only in the beginning of the process, these negative charges surrounding the solid tend to attract H^+ by raising the pH of the closest solution until the equilibrium is obtained. After that, the slower processes of dissolution, hydrolysis, etc. proceed, decreasing the pH.

The process is more complicated in volcanic ash due to the fact that, in addition to Si, there are also silicates of Na, Ca, K and Mg [34]. According to the studies on sodium feldspar by these authors, the process develops in three stages: (1) virtually instantaneous exchange of the alkaline ion by H^+ (or as (H_3O^+), i.e., with increase of pH; (2) generation and fast growth of a residual layer poor in that alkaline and rich in Si and/or Al (thicker at higher acidity); and (3) interaction of feldspar-solution through the residual layer (process necessarily slower, at pH lower than in previous steps).

The first stage involves a reversible reaction where H^+ forms the feldspar $HAlSi_3O_8$ when Na^+ is released. At the end of the second stage, a layer of this compound developed by incongruent dissolution. Similar results were obtained with a potassium-rich feldspar [35]. If there is enough time, the third stage, the slow one, controls the process of aqueous dissolution (weathering). This is the process that must have taken place on the batches studied here.

4.2.2. Ash reactivity

LOI (loss on ignition) values show that the studied ashes are relatively high in volatiles (Table 1a), but microscopy confirms no visible external particle weathering. The mineralogical and petrographic observations indicate that a significant portion of the ashes corresponds to anhydrous or slightly hydrated minerals. The biotite generally has less than 5% of H_2O, i.e., the whole-rock equivalent content is very low in the more micaceous samples (721, 733, and AS-28, Table 1a). Consequently, water should concentrate in the glass. Nevertheless, although the glass may contain halogens in very small quantities or traces, most of LOI is water and its content in glass should be somewhat higher than that indicated in Table 1a. This is significant because water is the main volatile controlling the explosive nature of the volcanic magma, which is the primary source of the ashes.

In essence, the dominant classical idea that water dissolves in silicate melts and reacts with the melts (highly polymerized) breaking the chains of the tetrahedral bonds (Si, Al)O_4 with oxygen, resulting two OH ends of two shorter chains by depolymerisation [36], implies that dissolved water appears in the network as (Si–OH) groups in chains smaller than those originated in a more anhydrous media. However, in the glass from such melts, spectroscopic investigations show that not only there are OH groups but there is also molecular H_2O, which has a specific role, though much more subordinate in depolymerisation. This coexistence and its effects are still unclear, but nevertheless some consistent inferences can be made.

The distribution of OH and water in the glass formed by melt quenching also reflects this distribution on melt, except at very high temperatures [37–39]. These works quantify the total amount of H_2O (H_2Ot), H_2O molecular (H_2Om) and OH in silicate glasses (natural and synthetic), cooled at high temperature, using infrared spectroscopy and point out the following conclusions of their results:

(1) The H_2Om appears from contents of $H_2Ot > 0.2\%$ shows a small increase up to 1% of H_2Ot, approximately, and grows more rapidly later, according to a regular variation. Probably, it is linked to the structure and is not a separate phase in inclusions or bubbles, as is clear from its absence in the studied spectra.
(2) The OH groups also grow regularly with the H_2Ot content. Unlike H_2Om, the increase of OH content is very fast up to 2–3% of H_2Ot, and then it slows down. Around 3% H_2Ot, water is distributed equally in H_2Om and OH. Once these values have been reached, H_2Om prevails increasingly on the OH content, although both increase (unevenly) with H_2Ot. That is, for low H_2Ot contents the hydroxyl groups are dominant over the H_2Om.
(3) The relationship $\%OH/\%H_2Om$ varies little with the chemical composition of glass from a melt cooled rapidly and varies nothing with pressure. However, this relationship increases moderately with the cooling temperature of glass [39]. As a guide, according to this author, the %OH in glasses with 2% H_2Ot, cooled at temperatures of 1000–200 °C, decreases steadily from 1.3 to 0.7%.

Applying these conclusions to present study and admitting temperatures cooling similar to the considered works [37,38], although all H_2Ot is not used in the depolymerisation, most of it must be because $(\%H_2Om/\%OH) < 1$. Only in the case of sample 808 the two percentages reverse this trend. In the other cases, the relationships are in the range of 0.4 to 0.8. At lower cooling temperatures, the percentage of OH is smaller but, as noted in (3), it is nevertheless remarkable. This, together with the intrinsic metastable character of the glass, points to an increase in reactivity when compared with the crystalline phases, facilitating hydrolysis. In general, natural glasses are less stable than crystalline minerals because the glass retains more energy from its parent magma than the latter minerals [40], being the dissolution rates significantly faster for Si-rich glasses than for their crystalline counterparts [41].

High ash reactivity not only depends on glass content but is a specially remarkable feature in ancient ashes, where the most labile

Table 5
Relative mass leached factors or RMLs (%) in nitric acid batches (nd, not determined).

Sample	719	721	733	808	809	AS-28	AS-29	AS-33
Ca	38.39	42.90	33.48	33.33	33.78	28.49	14.28	11.15
Mg	17.62	19.19	16.79	15.02	26.62	30.84	3.53	10.51
Na	0.68	1.14	1.76	8.62	5.10	1.17	2.51	9.68
K	0.68	1.19	1.05	1.42	1.05	1.28	1.64	8.78
Si	0.03	0.05	0.04	0.05	0.09	0.06	0.05	0.11
Li	1.67	2.81	1.72	9.14	8.83	3.02	7.62	19.18
Be	0.79	1.13	0.83	10.30	0.77	1.39	6.47	3.56
Al	0.55	0.81	0.41	2.19	0.80	1.00	0.61	2.67
P	95.48	63.67	88.48	52.58	96.14	92.18	79.38	97.04
Ti	2.01	0.97	1.36	0.54	5.59	6.38	1.12	3.99
V	5.29	4.51	7.95	12.67	27.31	20.40	2.06	4.33
Cr	5.86	4.01	3.61	19.56	25.33	17.19	2.26	4.08
Fe	4.38	5.72	5.11	4.16	9.66	14.50	1.60	4.99
Mn	3.97	7.66	3.03	13.17	6.29	7.99	4.43	8.39
Co	23.68	17.82	46.09	88.84	2.57	2.05	61.19	77.95
Ni	90.11	48.69	58.30	75.48	84.24	52.95	17.72	30.45
Cu	17.75	24.48	25.19	21.03	42.91	26.68	5.98	19.20
Zn	96.57	76.47	94.32	62.44	95.15	38.74	33.47	61.93
Ga	0.69	1.08	0.59	1.49	1.18	1.69	0.94	4.10
Ge	<0.01	0.04	<0.01	0.45	0.34	0.13	0.19	1.44
As	17.09	23.74	16.69	18.59	7.83	28.50	57.39	77.69
Rb	0.74	1.16	0.63	1.85	0.80	1.06	4.83	18.69
Sr	19.76	12.76	12.02	18.14	17.35	9.86	1.07	4.43
Y	2.21	6.91	3.12	8.74	3.63	4.63	8.58	11.67
Zr	0.56	0.77	0.43	1.06	1.11	0.81	3.39	1.47
Nb	0.15	0.12	0.09	0.73	0.39	0.47	0.57	0.62
Mo	16.46	14.08	12.51	11.37	15.33	14.01	16.73	19.30
Sn	nd	nd	nd	2.48	1.64	0.49	nd	0.10
Sb	11.16	6.76	6.90	41.84	13.68	4.51	1.17	3.71
Cs	0.93	1.40	1.59	7.41	0.60	1.37	6.60	50.17
Ba	18.79	12.03	15.86	5.62	12.37	4.91	1.09	4.08
La	3.76	9.91	6.41	8.31	6.24	7.87	7.16	18.79
Ce	3.39	9.69	6.21	9.58	5.62	7.61	7.12	17.92
Pr	1.35	10.93	6.86	9.14	5.94	8.21	7.60	16.41
Nd	4.42	12.01	7.44	9.79	6.61	9.25	7.33	15.59
Sm	2.15	11.28	6.59	9.99	5.79	8.61	6.18	13.19
Eu	1.93	13.92	10.37	9.41	11.11	12.96	3.20	7.55
Gd	4.23	11.40	6.50	9.90	6.06	8.11	5.96	13.31
Tb	1.55	9.82	5.12	10.03	5.32	6.67	5.40	11.54
Dy	3.29	8.72	4.27	9.06	4.46	6.06	5.41	9.98
Ho	1.28	7.32	3.26	8.58	3.70	4.81	5.45	8.74
Er	2.41	6.34	2.77	8.34	3.23	4.42	5.06	8.47
Tm	0.88	4.94	2.02	7.75	2.62	2.78	5.32	7.44
Yb	1.84	3.87	1.70	8.11	2.23	2.53	5.43	7.71
Lu	0.63	3.64	1.52	7.51	1.91	2.09	5.52	8.47
Hf	0.91	1.17	0.65	5.92	7.88	1.67	2.44	6.50
Ta	0.18	0.16	0.17	3.38	0.95	0.20	0.56	1.73
Tl	0.70	1.98	1.03	2.52	1.45	3.23	2.34	23.14
Pb	2.42	3.61	2.14	11.51	2.78	3.25	1.85	15.83
Bi	2.48	2.20	1.88	6.54	2.00	2.92	6.82	23.82
Th	1.06	1.94	0.68	4.08	1.19	1.09	6.38	7.26
U	0.46	1.02	0.28	2.26	0.65	0.33	7.11	5.86

elements, such as those showing preferential enrichment on tephra surfaces (e.g., SO_4^{2-}, Cl^- and F^-), were probably released during the early burial of the deposit. As a result, the role of glass in the release of major, minor and trace elements is potentially greater in ancient ashes than in current ones.

4.2.3. Element mobility

Once determined the relative mass leached factors (RMLs) for each element (Table 4), the elements were grouped according to their mobility expressed by their RML:

(1) High mobile elements (RML > 5%): P, Zn, Sb, Cu, and Ni.
(2) Moderate mobile elements (RML between 0.5 and 5%): Ca, Mg, Na, As, Ba, Co, Cr, Hf, Li, Mo, Sr, and V.
(3) Low mobile elements (RML < 0.5%): Si, Al, Fe, Mn, Ti, Be, Cs, Ga, Ge, Nb, Pb, Rb, Sn, Ta, Th, Tl, U, Y, Zr, and REE.

This classification must be taken with caution because it is a generalization. Although in a more detailed classification some elements would appear in more than one class, they are included here in the most common group. An extreme case is As. It has been concluded as a moderate mobile element in this general classification, but in reality it occurs as a high mobile element (samples AS28 and AS33), moderate mobile element (719, 721, 809), and low mobile element (733, 808, AS29). Moreover, the above classification is unreliable for elements with concentrations close to their detection limits.

It is well established that silicon, the most abundant major element in volcanic ash, has a slightly decreasing solubility with increasing pH in the acidic range, increasing strongly from pH 9 and having a slightly accentuated minimum toward neutrality (pH 7–8), at around 55 mg l^{-1} of Si [42]. Sample AS-29 nearly reaches this saturation at this pH, which demonstrates the magnitude of experimental leaching despite the low mobilization RML observed (Table 4).

In general, the most immobile major elements considered in the weathering processes are Al and Fe (solubility products of their hydroxides are extremely low, 10^{-33} and 10^{-39}, respectively) [43,44]. This is not always observed in the studied samples. The molar ratio Si/Al in rock (Table 1a) is clearly lower than in the aqueous leachate (Table 2a), except for sample 808 (which is only slightly lower), and sample AS-33, where the terms are reversed and Si/Al is higher in rock than in water. This implies that Al dissolves more readily than Si in this ash. Some relatively high values for Fe, Ti, and geochemically analogous elements were also observed in concentrations with orders of magnitude of tens to hundreds of $\mu g\,l^{-1}$. The explanation of these anomalies is found that these elements can occur as stable complexes which may be dissolved in these conditions. Such complexes are clearly dependent on pH.

The behaviour of Ca, Mg, Na and K corresponds to moderate mobility. The RML is higher for Ca and Na, probably because the silicates bearing these two elements are very susceptible to weathering. The mobility of K, although low, is larger than that of the alkaline-linked elements, with higher ionic radius, Rb and Cs. The Sr, with a larger mobility than the latter, follows a behaviour closer to Ca and Na. Finally, Li behaves more like Na than K.

The case of P is peculiar, with high RMLs, approaching 100% in one case (sample 809, Table 4). This element typically concentrates in a single mineral – apatite – in high silica igneous rocks, although it can occasionally appear in others (monazite, xenotime, Li phosphates, etc.), and also within the network of alkali aluminium silicates (see below). It has long been established that P is somewhat easily mobilized in the weathering of rocks considered here, according to their mineralogical variety [45,46]. Its dissolution at different pH values has been investigated experimentally [47]. The behaviour of apatite in the weathering of igneous rocks with high silica content was studied in detail by electron microscopy by Banfield and Eggleton [48], who found that weathering mobilized early not only around 85% of the existing P of the original rock, but also REE and Y. They identified four mineral phases replacing apatite, phosphates of Al and REE (florencite, rhabdophane, etc.), which may also be dissolved during weathering. Finally, all studied weatherings solubilise phosphorus, but in some cases this process occurs early on and in others, much later, depending on the variety of apatite [45].

The less mobile minor and trace elements on the water batches were Ti, Be, Cs, Ga, Ge, Nb, Pb, Rb, Sn, Ta, Th, Tl, U, Y, Zr, and REE (Table 4), which are nearly all well characterized as less mobile in weathering processes. The exceptions are sample AS-29 and, especially, AS-33, the most ferromagnesian and with lower silica content ashes (Table 1a). In these two samples, these elements are mobilized than in the rest, though more limitedly. The contents are normal in such materials: a bit less Si, K, Rb, Cs, etc., and something more Ca, Ti, Sr, Zr, etc. Therefore, this behaviour must be related to: (1) a better feasibility for hydrolysis of these rocks compared with those with higher silica and lower ferromagnesian contents (a well-known feature); and (2) a lower retention capacity, either produced by the lack of external ions that could improve solubility and/or by the not yet well-developed surface features that facilitate the adsorption of the most favourable elements (with high-alkali ionic radius and low charge, among others).

As for the REE, with low mobility as a group, stands again samples AS-29 and AS-33 stand out, having a different REE pattern than the others. This is probably due to the fractionation of REE during hydrolysis (see above the case of P). These elements, besides appearing in apatite in rocks derived from high silica magmas, can concentrate also in allanite, titanite, zircon, monazite and xenotime. Because these five minerals are much more resistant to weathering, the presence of apatite is probably what controlled the leaching. Samples AS-33 and 733 have the highest RML values for Ce, probably because that medium is more reductive: Ce^{3+} is much more soluble than Ce^{4+}.

The trace elements with the highest mobility were Zn, Sb, Cu, and Ni. The first two seem to have similar behaviour, as do the two latter. The weathering of easily alterable minerals such as sulphides and/or biotite could explain these features.

4.3. Comparison between water and nitric acid batches

Logically, in general, leaching is stronger with an acid than with water (Tables 2a and 2b and Tables 3a and 3b). The mobility of elements in the acid batch, compared with those in water, is clearly higher. The exceptions were Si and Ge. Once determined the RMLs for each element, they were grouped according to their mobility in the nitric acid batches, expressed by their RML:

(1) High mobile elements (RML > 5%): Ca, Mg, Fe, Mn, P, As, Ba, Co, Cu, Mo, Ni, Sb, Sr, V, Y, Zn, and REE.
(2) Moderate mobile elements (RML between 0.5 and 5%): Na, K, Al, Ti, Be, Bi, Bi, Cr, Cs, Ga, Hf, Li, Nb, Pb, Rb, Sn, Ta, Th, Tl, U, and Zr.
(3) Low mobile elements (RML < 0.5%): Si and Ge.

A special case is Si, whose concentration is lower in the acid batch than in the water batch. Boron also shows a somewhat similar behaviour although the concentration range is much lower. In order to compare the values in Tables 2a and 2b (water) with those of Tables 3a and 3b (nitric acid), the figures in Tables 2a and 2b should be multiplied by 5 (0.1 g of ash were used in both cases but with 5 ml of water in the first batch and 1 ml of nitric acid in the second). This comparison shows that the Si concentration extracted with water is 2–5 times higher than those with HNO_3, sample AS-29 being 17 times higher. That is, the stronger the attack the less concentration of Si (Table 3a).

This feature can be justified based on the classical experimental studies on the solubility of a type of amorphous silica in nitric acid of different normality (N) at temperatures between 36 and 95 °C [49]. For a given temperature, the solubility varies according to the equation:

$$\log C = K_1 N + K_2$$

where K_1 and K_2 are constants (both of negative value) at such temperature, N is the normality of the nitric acid, and C the dissolved silica concentration. The silica solubility for the nitric acid batches used in our study was estimated indicatively extrapolating the results of these authors at 20 °C, bearing in mind that the experiment was performed using $14.34N$ HNO_3. Hence, the equation obtained for the temperature of the experience and the Si concentration expressed as $mg\,l^{-1}$ is

$$\log[\mathrm{Si}] = -0.211N + 1.724$$

Therefore, the solubility obtained for the nitric acid batch is $0.05\,mg\,l^{-1}$ of Si, a value 10 times lower than the solubility of $55\,mg\,l^{-1}$ of Si in water at circumneutral pH [42]. In other words, precipitated silica is generated during acid treatment.

The analytical method used justified the apparent contradiction that the acidic batch contained higher silicon than its solubility limit. Indeed, the nitric acid solution was filtered at 0.45 μm. Successive washings of the unfiltered waste with water may have solubilised some silica (not all). In the retained fraction, in addition to the precipitated silica, there was also polymerized silica, colloidal, with tiny 1 μm micelles [50]. It is well known that this silica can hold small amounts of other elements (Al, Fe, Ti, Ge, etc.), either by adsorption, solid solution or occlusion, a feature that can irregularly affect the distribution of components.

With the exception of Si, the behaviour of the rest of the elements can be explained in the same way as for the water batches. The high concentration extracted in the nitric acid batches for Zn – in many cases with a recovery of close to 100% – suggests that this element is more associated with sulphides, which are more easily weathered, than with silicates. The difference of Zn with Cu and Pb, with which it is often associated, seems to indicate that the latter are related to the silicates.

Although there are no available analytical results on sulphide ion, but on total sulphur, expressed as sulphate, it is very likely that it exists in these samples. There is a clearly higher sulphate content in the nitric acid than in the water batches (Table 3a). It is logical that acid leaching dissolves all existing S compounds better; however, such high figures suggest that nitric acid, a strong oxidizer, is also oxidizing sulphur compounds of lower valence, including sulphides. By given the experimental procedure (different dilution in aqueous and nitric acid batches), the ratio between sulphur in a nitric acid leachate (S_n) and sulphur in an aqueous leachate (S_w) has been calculated (Table 3a). This relationship (S_n/S_w) varies largely among samples, suggesting that sulphur may be present as S^{2-}.

Again is illustrative the case of P. This element is usually concentrated as phosphate, mainly as apatite (the most leachable in water), although there may be others, already mentioned, more scarce and resistant, that also can be found in silicates. As observed earlier, sample 809 leached practically all its P in the nitric acid media, confirming that it is in fact phosphate. On the other hand, only a P fraction is solubilised in the other samples in the acidic media, suggesting that P is also in a more resistant network of silicate. The presence of phosphorus in the feldspar network is well known. This element displays an affinity for alkalis and Al, not for Si, in water saturated rhyolitic melts [51]. The accumulation of P in alkali feldspar increases with the excess of Al, expressed by the alumina saturation index A/CNK. The sample with lower leachable P in HNO_3, sample 808 (Table 3b), is the only peraluminous composition, with an A/CNK index of 1.09 (Table 1a). Therefore, almost 50% of P must be in the silicate network.

The concentrations of Be, V, Cr, and Mo appear unaffected by large variations in acidity and alkalinity, suggesting a high solubility for these transition metals in these solvents. The hypothesis drawn from these results is that these cations are dominantly combined with halogens and sulphate as metal salts and aerosols adsorbed to particle surfaces. It is supported by studies of trace metals in the gaseous phase at several volcanoes [2,8,52,53].

4.4. Environmental concerns

The environmental concerns of the studied volcanic ash deposits are mainly related to the presence of fine grain-size fractions (health risk by inhalation), and the chemical hazard when there is interaction with water. The former case is more dangerous if the presence of cristobalite is confirmed as one-dimensional crystalline silica nanostructures, as in the ash of the Chaiten Volcano [31].

Although the ashes are from an arid region in northwestern Argentina where the average precipitation rarely exceeds 200 mm per year, the interaction of ashes with water is a very important environmental concern for the changes in pH levels as well as for the potential toxicity of ash-leachates, increasing ecosystem stress [2,6]. If the deposits are exposed to water, subsequent leaching and transport in surface and groundwater could have the potential to induce biogeochemical stress.

The minor and trace elements presenting the most significant load in water batches, ordered from higher to lower concentrations, include Al > B > Fe > Zn > F > P > Mn > Ba > Sr > Li > Ti > Rb > Cu > Ni > Sb > Pb > As > Cr > V (Table 2b). The sample of ash with the most leaching potential was AS-33.

From the point of view of drinking water, certain previously mentioned elements appear in quality guidelines due to their potential toxicity [54,55]. These elements are Al, As, B, Ba, Cr, Cu, F, Fe, P, Mn, Mo, Ni, Pb, Sb, and Zn.

The volume of the studied deposits is relatively small because they represent blankets, very discontinuous on the Earth's surface, of some tens of centimetres of thickness. Nevertheless, the leachate drainage in small and closed hydrographic basins such as the ones in the Puna and surrounding regions can greatly affect the geochemical fluxes of streams and lakes, especially immediately after the scarce rainfalls, because the process is very fast. Thus, ecosystem stresses are expected after strong rainfalls.

5. Conclusions

Ashes from the Puna and surrounding areas in northern Argentina demonstrate that sometimes volcanic ash deposits are very well preserved (up to several million years), maintaining a potential hazard for the environment in the same way as recent ones.

The finest fractions of the ashes could represent a hazard by inhalation. Furthermore, local geochemical fluxes can vary due to ash–water interaction. This interaction produces fast changes, mainly in pH and in the release of potentially toxic trace elements (PTTE).

From a methodological point of view, SEM–EDX examination is a powerful tool to identify and characterize, both compositionally and morphologically, the particles contained in the ash. The combination of this preliminary examination with DRX analyses and leaching batches clearly highlight the main environmental concerns related to the studied ashes. The water-batch tests were extremely useful, and showed very satisfactory results, for the study of geochemical fluxes derived from ash-natural water interaction. The nitric acid batches confirm these results but have the disadvantage to precipitate silica, which could disturb the distribution of other elements (e.g., Al, Fe, Ti, Ge). Hence, the water batches are recommended for ash leachate characterization.

The high reactivity of ashes is associated with the high content of natural glass, the most important component of this material, inducing very fast changes in pH and released element contents during leaching. The geological processes implied in high-silica explosive eruptions, sources of the studied ashes, vary little from one eruption to another. Bearing in mind that two of the studied samples are probably from the same eruption, the cluster of elements released is very close in terms of element and content, such as: Al > B > Fe > Zn > F > P > Mn > Ba > Sr > Li > Ti > Rb > Cu > Ni > Sb > Pb > As > Cr > V. The ash–water interaction, although scarce in arid regions such as the Puna in northern Argentina, introduces fast changes in the geochemical fluxes of elements and pH, and it could be a potential hazard for the environment. In fact, many of the mentioned elements are included in the drinking water guidelines for their potential toxicity or harmful properties (Al, As, B, Ba, Cr, Cu, F, Fe, P, Mn, Mo, Ni, Pb, Sb, and Zn). To minimize these hazards it is recommended to avoid the input on water supply systems from water resources affected by ash leaching immediately after a strong rainy event.

Acknowledgements

We acknowledge the technical support of ICTJA DRX Survey (J. Elvira) and the Scientific-Technical Surveys of the University of Barcelona in the analytical work. This study was carried out in the framework of the PEGEFA Working Group (Catalonian Government "Grup de Recerca Consolidat" SGR-2005-00795 and 2009-SGR-

972), and was partly funded by the Project ASH of the Spanish Ministry of Science and Technology (CGL2008-00099) and the FPU Grant of the Spanish Ministry of Education of one of the authors (F. Ruggieri, Ref. AP2006-04592). The English of the final draft of the manuscript was improved by Frances Luttikhuizen. We are grateful to Dr. Tahir Rafique and an anonymous reviewer for the care with which they reviewed the original manuscript.

References

[1] R. Schmid, Descriptive nomenclature and classification of pyroclastic deposits and fragments—recommendations of the IUGS subcommission on the systematics of igneous rocks, Geology 9 (1981) 41–43.
[2] M.T. Jones, S.R. Gislason, Rapid releases of metal salts and nutrients following the deposition of volcanic ash into aqueous environments, Geochimica et Cosmochimica Acta 72 (2008) 3661–3680.
[3] M.A. Armienta, S. De la Cruz-Reyna, O. Morton, O. Cruz, N. Ceniceros, Chemical variations of tephra-fall deposit leachates for three eruptions from Popocatepetl volcano, Journal of Volcanology and Geothermal Research 113 (2002) 61–80.
[4] M.A. Armienta, A.L. Martin-Del-Pozzo, R. Espinasa, O. Cruz, N. Ceniceros, A. Aguayo, M.A. Butron, Geochemistry of ash leachates during the 1994–1996 activity of Popocatepetl volcano, Applied Geochemistry 13 (1998) 841–850.
[5] F. Risacher, H. Alonso, Geochemistry of ash leachates from the 1993 Lascar eruption, northern Chile, implication for recycling of ancient evaporites, Journal of Volcanology and Geothermal Research 109 (2001) 319–337.
[6] C.S. Witham, C. Oppenheimer, C.J. Horwell, Volcanic ash-leachates: a review and recommendations for sampling methods, Journal of Volcanology and Geothermal Research 141 (2005) 299–326.
[7] P. Allard, A. Aiuppa, H. Loyer, F. Carrot, A. Gaudry, G. Pinte, A. Michel, G. Dongarra, Acid gas and metal emission rates during long-lived basalt degassing at Stromboli volcano, Geophysical Research Letters 27 (2000) 1207–1210.
[8] P. Delmelle, M. Lambert, Y. Dufrene, P. Gerin, N. Oskarsson, Gas/aerosol–ash interaction in volcanic plumes: new insights from surface analyses of fine ash particles, Earth and Planetary Science Letters 259 (2007) 159–170.
[9] N. Oskarsson, The interaction between volcanic gases and tephra—fluorine adhering to tephra of the 1970 Hekla eruption, Journal of Volcanology and Geothermal Research 8 (1980) 251–266.
[10] W.I. Rose, Scavenging of volcanic aerosol by ash—atmospheric and volcanologic implications, Geology 5 (1977) 621–624.
[11] J.C. Varekamp, J.F. Luhr, K.L. Prestegaard, The 1982 eruptions of El-Chichon volcano (Chiapas, Mexico)—character of the eruptions, ash-fall deposits, and gas-phase, Journal of Volcanology and Geothermal Research 23 (1984) 39–68.
[12] P Frogner, S.R. Gislason, N. Oskarsson, Fertilizing potential of volcanic ash in ocean surface water, Geology 29 (2001) 487–490.
[13] M. Garcia-Vallés, J.L. Fernandez-Turiel, D. Gimeno, S.J.F. Ruggieri, Los yardangs del Campo de Piedra Pómez, Catamarca, Argentina, Geo-Temas 10 (2008) 1353–1356.
[14] C.R. Stern, Active Andean volcanism: its geologic and tectonic setting, Revista Geologica de Chile 31 (2004) 161–206.
[15] S.L. de Silva, P.E. Francis, Volcanoes of the Central Andes, Springer-Verlag, New York, 1991.
[16] M.M. Soler, P.J. Caffe, B.L. Coira, A.T. Onoe, S.M. Kay, Geology of the Vilama caldera: a new interpretation of a large-scale explosive event in the Central Andean plateau during the Upper Miocene, Journal of Volcanology and Geothermal Research 164 (2007) 27–53.
[17] R.S. Thorpe, P.W. Francis, Variations in andean andesite compositions and their petrogenetic significance, Tectonophysics 57 (1979) 53–70.
[18] A. Risse, R.B. Trumbull, B. Coira, S.M. Kay, P. van den Bogaard, Ar-40/Ar-39 geochronology of mafic volcanism in the back-arc region of the southern Puna plateau, Argentina, Journal of South American Earth Sciences 26 (2008) 1–15.
[19] O. Ersoy, G. Chinga, E. Aydar, A. Gourgaud, H.E. Cubukcu, I. Ulusoy, Texture discrimination of volcanic ashes from different fragmentation mechanisms: a case study, Mount Nemrut stratovolcano, eastern Turkey, Computers & Geosciences 32 (2006) 936–946.
[20] G Heiken, K.H. Wohletz, Volcanic Ash, second ed., University of California Press, Berkeley, California, 1992.
[21] K.P. Severin, Energy Dispersive Spectrometry of Common Rock Forming Minerals, Kluwer Academic Publishers, 2004.
[22] N. Imai, S. Terashima, S. Itoh, A. Ando, 1994 compilation values for GSJ reference samples, igneous rock series, Geochemical Journal 29 (1995) 91–95.
[23] S. Terashima, S. Itoh, M. Ujiie, H. Kamioka, T. Tanaka, H. Hattori, 3 new GSJ rock reference samples—rhyolite JR-3, gabbro JGB-2 and hornblendite JH-1, Geostandards Newsletter 17 (1993) 1–4.
[24] J.L Fernandez-Turiel, J.F. Llorens, M. Carnicero, F. Valero, Application of ICP-MS to outlet water control in the Llobregat and Ter drinking water treatment plants, Quimica Analitica 19 (2000) 217–224.
[25] J.L. Fernandez-Turiel, J.F. Llorens, F. Lopez-Vera, C. Gomez-Artola, I. Morell, D. Gimeno, Strategy for water analysis using ICP-MS, Fresenius Journal of Analytical Chemistry 368 (2000) 601–606.
[26] J.L. Fernandez-Turiel, A. López, J.F. Llorens, X. Querol, P. Aceñolaza, F. Durand, J.P. López, M.E. Medina, J.N. Rossi, A.J. Toselli, J. Saavedra, Environmental monitoring using surface water, riversediments, and vegetation: a case study in the Famatina Range, La Rioja, NW Argentina, Environment International 21 (1995) 807–820.
[27] C.M. Bethke, Geochemical and Biochemical Reaction Modeling, Cambridge University Press, New York, 2008.
[28] A. Georgakopoulos, A. Filippidis, A. Kassoli-Fournaraki, Leachability of major and trace elements of fly ash from Ptolemais power station, Northern Greece, Energy Sources 24 (2002) 103–113.
[29] A. Georgakopoulos, A. Filippidis, A. Kassoli-Fournaraki, A. Iordanidis, J.L. Fernandez-Turiel, J.F. Llorens, D. Gimeno, Environmentally important elements in fly ashes and their leachates of the power stations of Greece, Energy Sources 24 (2002) 83–91.
[30] M.J. Le Bas, R.W. Le Maitre, A. Streckeisen, B. Zanettin, A chemical classification of volcanic rocks based on the total alkali-silica diagram, Journal of Petrology 27 (1986) 745–750.
[31] M. Reich, A. Zuniga, A. Amigo, G. Vargas, D. Morata, C. Palacios, M.A. Parada, R.D. Garreaud, Formation of cristobalite nanofibers during explosive volcanic eruptions, Geology 37 (2009) 435–438.
[32] P.J. Baxter, C. Bonadonna, R. Dupree, V.L. Hards, S.C. Kohn, M.D. Murphy, A. Nichols, R.A. Nicholson, G. Norton, A. Searl, R.S.J. Sparks, B.P. Vickers, Cristobalite in volcanic ash of the Soufriere Hills Volcano, Montserrat, British West Indies, Science 283 (1999) 1142–1145.
[33] G.A. Parks, Surface energy and adsorption at mineral-water interfaces: an introduction, in: M.F. Hochella, A.F. White (Eds.), Reviews in Mineralogy—Mineral–Water Interface Geochemistry, Mineralogical Society of America, Washington, 1990, pp. 133–175.
[34] R. Wollast, L. Chou, Surface-reactions during the early stages of weathering of albite, Geochimica et Cosmochimica Acta 56 (1992) 3113–3121.
[35] G.R. Holdren, P.M. Speyer, pH dependent changes in the rates and stoichiometry of dissolution of an alkali feldspar at room-temperature, American Journal of Science 285 (1985) 994–1026.
[36] D.B Dingwell, Recent experimental progress in the physical description of silicic magma relevant to explosive vulcanism, in: J.S. Gilbert, R.S.J. Sparks (Eds.), The Physics of Explosive Volcanic Eruption, Geological Society, Special Publications, London, 1998, pp. 9–26.
[37] P.D. Ihinger, Y.X. Zhang, E.M. Stolper, The speciation of dissolved water in rhyolitic melt, Geochimica et Cosmochimica Acta 63 (1999) 3567–3578.
[38] E.M. Stolper, Water in silicate glasses: an infrared spectroscopic study, Contribution to Mineralogy and Petrology 81 (1982).
[39] E.M. Stolper, Temperature dependence of the speciation of water in ryolitic melts and glasses, American Mineralogist 74 (1989) 1247–1257.
[40] A. Stefánsson, S.R. Gíslason, S. Arnórsson, Dissolution of primary minerals in natural waters II. Mineral saturation state, Chemical Geology 172 (2001) 251–276.
[41] D. Wolff-Boenisch, S.R. Gislason, E.H. Oelkers, The effect of crystallinity on dissolution rates and CO2 consumption capacity of silicates, Geochimica et Cosmochimica Acta 70 (2006) 858–870.
[42] G.B. Alexander, W.M. Heston, R.K. Iler, The solubility of amorphous silica in water, Journal of Physical Chemistry 58 (1954) 453–455.
[43] K.H. Gayer, L.C. Thompson, O.T. Zajicek, The solubility of aluminum hydroxide in acidic and basic media at 25 °C, Canadian Journal of Chemistry-Revue Canadienne De Chimie 36 (1958) 1268–1271.
[44] J.C. Chang, Solubility product constants, in: D.R. Lide (Ed.), CRC Handbook of Chemistry and Physics, The Chemical Rubber Co, Boca Raton, 1999.
[45] J.J. Middelburg, C.H. Vanderweijden, J.R.W. Woittiez, Chemical processes affecting the mobility of major, minor and trace-elements during weathering of granitic-rocks, Chemical Geology 68 (1988) 253–273.
[46] C.M Rice, Chemical weathering on Carnmenellis granite, Mineralogical Magazine 39 (1973) 429–447.
[47] E. Nickel, Experimental dissolution of light and heavy minerals in comparison with weathering and intrastratal dissolution, Contributions to Sedimentology 1 (1973) 1–68.
[48] J.F. Banfield, R.A. Eggleton, Apatite replacement and rare-earth mobilization, fractionation, and fixation during weathering, Clays and Clay Minerals 37 (1989) 113–127.
[49] T.H Elmer, M.E. Nordberg, Solubility of silica in nitric acid solutions, Journal of the American Ceramic Society 41 (1958) 517–520.
[50] R.K. Iler, Isolation and characterization of particle nuclei during the polymerization of silicic-acid to colloidal silica, Journal of Colloid and Interface Science 75 (1980) 138–148.
[51] D. London, G.B. Morgan, H.A. Babb, J.L. Loomis, Behavior and effects of phosphorus in the system Na_2O–K_2O–Al_2O_3–SiO_2–P_2O_5–H_2O at 200 MPa(H2O), Contributions to Mineralogy and Petrology 113 (1993) 450–465.
[52] F. Africano, G. Van Rompaey, A. Bernard, F. Le Guern, Deposition of trace elements from high temperature gases of Satsuma-Iwojima volcano, Earth Planets and Space 54 (2002) 275–286.
[53] A. Bernard, F. Leguern, Condensation of volatile elements in high-temperature gases of Mount St. Helens, Journal of Volcanology and Geothermal Research 28 (1986) 91–105.
[54] ANMAT (Administración Nacional de Medicamentos Alimentos y Tecnología Médica), Código Alimentario Argentino (CAA)-Capitulo XII—Bebidas Hídricas, Agua y Agua Gasificada-Agua Potable, 2007.
[55] WHO (World Health Organization), Guidelines for Drinking Water Quality, First addendum to third edition volume 1 Recommendations, 2006.